ELSEVIER

Polymer 41 (2000) 4825–4830

polymer

Microgel formation in high molecular weight poly(ethyleneoxide)

S. Rangelov[1], W. Brown*

Department of Physical Chemistry, University of Uppsala, Box 532, 751 21 Uppsala, Sweden

Received 7 July 1999; accepted 21 September 1999

Abstract

Light scattering measurements show that, below molecular weights of about 10^6, PEO chains in aqueous solution follow the expected pattern of behavior for a flexible chain in a thermodynamically good solvent, although the coils are unusually extended because of specific interactions with water. For higher molecular weight chains, the molecular weight scaling exponent for the radius of gyration decreases and the parameter $\rho = (R_g/R_h)$ consequently decreases. The observed collapse to a more compact coil conformation is because of microgel formation, probably stabilized by intramolecular hydrogen bonding via solvent molecules.

Keywords: Polyethyleneoxide; Coil–coil interactions; Light scattering

1. Introduction

Much of the literature on polyethyleneoxide (PEO) in aqueous solution has been concerned with materials of molecular mass less than about 10^6. For these materials, it is the general consensus that the single chain behavior is typical of a flexible chain in a thermodynamically good solvent, although the PEO coil is clearly larger and the coil–coil interactions are stronger than is normally the case for flexible chains in good solvent systems. It was speculated [1,2] that this may be because of the way that water can be arranged within the coil, coupled with the packing of water at the ether links of the chain backbone.

Another aspect of dilute PEO solutions is the ubiquitous presence of aggregates that are observable in dynamic light scattering measurements as a slowly relaxing diffusive component of high relative intensity with a hydrodynamic radius in excess of 100 nm. It has been concluded that the aggregates are ultimately attributable to the presence of hydrophobic impurities, probably deriving from the mode of synthesis, and that they can be removed from the dilute solutions using hydrophobic filters or appropriate small pore diameter filters. Alternatively, one can speculate on the importance of intermolecular hydrogen bonding involving the ether oxygens. Such aggregates yielding a high polydispersity (together with the well-known degradation of PEO in aqueous solutions with time) frequently complicate the interpretation of the solution properties of PEO polymers. We have directed our attention to high molecular mass samples of PEO in order to further elucidate the solution properties of this important polymer.

2. Experimental

2.1. Materials

Six commercial samples of PEO with viscometric molecular weights in the range $0.3–8.0 \times 10^6$, according to Union Carbide (Table 1) were used without further purification.

2.2. Solution preparation

Four to six aqueous solutions of each PEO fraction in the concentration range below $0.8C^*$, where $C^*(= 1/[\eta])$ is the overlap concentration, were prepared by the dilution of stock solutions. The solutions of each polymer were prepared by dissolving the appropriate amount of polymer in purified water (Millipore Super-Q-System). The diluted solutions were filtered directly into dust-free light scattering cells using 0.45 μm Millipore Sartorius Minisart filters (cellulose acetate membranes). Concentrations are expressed throughout as *C*g/ml.

2.3. Methods

2.3.1. Light scattering

The light scattering setup consists, as described previously [3] of a 488 nm Ar ion laser and the detector

* Corresponding author.

[1] Permanent address: Institute of Polymers, Bulgarian Academy of Sciences, 1113 Sofia, Bulgaria.

0032-3861/00/$ - see front matter
PII: S0032-3861(99)00708-9

Table 1
Viscosimetric molecular weights of high molecular weight PEO samples

Sample	N750	N12K	N60K	WSR 301	WSR	309
$10^{-6} M_\eta$	0.30	1.0	2.0	4.0	5.0	8.0

optics with an ITT FW 130 photomultiplier and ALV-PM-PD amplifier-discriminator connected to an ALV-5000 autocorrelator built into a computer. The cylindrical scattering cells were sealed and then immersed in a large-diameter thermostated bath containing the index-matching fluid decalin. Measurements were made at different angles in the range 30–140°, and at different sample concentrations. Information on the molecular weight, the radius of gyration, and the second virial coefficient was obtained from the dependence of the reduced scattered intensity KC/R_θ on the concentration (C) and the scattering angle (θ) measured in the simultaneous static and dynamic experiment. $K = (4\pi^2 n^2/N_A\lambda^4)\,(dn/dC)^2$. Toluene was used as the reference scatterer ($R_{ref} = 4.0 \times 10^{-7} m^{-1}$ at $\lambda = 488$ nm). N_A is Avogadro's constant and λ the wavelength. The refractive index increment (dn/dC) was measured in a differential refractometer with Rayleigh optics. For the present system, $dn/dC = 0.131.10^{-3}$ dm^3 g^{-1} at the wavelength used and 25°C. The Rayleigh ratio was determined as $R_\theta = [(I - I_0)/I_{ref}]R_{ref}(n/n_{ref})^2$. Here $n = 1.33$ is the solvent refractive index and n_{ref} that of toluene. I is the measured total time-averaged scattered intensity, I_0 that of the solvent, water, and I_{ref} that of toluene.

Analysis of the dynamic data was performed by fitting the experimentally measured $g_2(t)$, the normalized intensity autocorrelation function, which is related to the electrical field correlation function $g_1(t)$ by the Siegert relationship [4]:

$$g_2(t) - 1 = \beta|g_1(t)|^2 \tag{1}$$

where β is a factor accounting for deviation from ideal correlation. For polydisperse samples, $g_1(t)$ can be written as the inverse Laplace transform (ILT) of the relaxation time distribution, $\tau A(\tau)$ [5]:

$$g_1(t) = \int \tau A(\tau) \exp(-t/\tau)\, d \ln \tau \tag{2}$$

where t is the lag-time. The relaxation time distribution, $\tau A(\tau)$, is obtained by performing ILT using the constrained regularization algorithm REPES [3], which minimizes the sum of the squared differences between the experimental and calculated $g_2(t)$. A mean diffusion coefficient D is calculated from the second moment of each peak as $D = \Gamma/q^2$, where q is the magnitude of the scattering vector $q = (4\pi n/\lambda)\sin(\theta/2)$ and $\Gamma = 1/\tau$ is the relaxation rate of each mode. Here θ is the scattering angle, n the refractive index of the medium and λ the wavelength of the light in vacuum.

Within the dilute regime, D varies linearly with the concentration according to:

$$D = D_0(1 + k_D C + \cdots) \tag{3}$$

where D_0 is the diffusion coefficient at infinite dilution and k_D is the hydrodynamic "virial" coefficient related to the second virial coefficient A_2 by:

$$k_D = 2A_2M - k_f - 2v_2. \tag{4}$$

Here M is the molar mass, k_f defines the concentration dependence of the friction coefficient in $f = f_0(1 + k_f C + \cdots)$ and v_2 is the partial specific volume.

The Stokes–Einstein equation relates D_0 to the hydrodynamic radius (R_h):

$$R_h = kT/(6\pi\eta D_0) \tag{5}$$

kT is the thermal energy factor and η is the temperature-dependent viscosity of water.

3. Results and discussion

3.1. Static light scattering parameters

Weight-average molecular weights, radii of gyration, and second virial coefficients were determined by double extrapolation of KC/R_θ to zero angle and concentration where K and R_θ are defined in Section 2. Typical static light scattering plots for PEO sample WSR ($M_w = 2.2 \times 10^6$) are shown in Fig. 1a and b. As seen in Fig. 2, the second virial coefficients for the different samples were somewhat erratic, falling to a very low value for the highest molecular mass. The dotted line in Fig. 2 has the theoretical slope of −0.2.

3.2. Dynamic parameters

Following filtration through the 0.45 μm filters, it was possible to examine the single coil behavior of high molar mass PEO in the absence of large aggregates. An example of a correlation function and the corresponding relaxation time distribution is shown in Fig. 3a and b for sample WSR ($M_w = 2.2 \times 10^6$). Intensity autocorrelation functions were analyzed by REPES yielding distributions of relaxation time. The distributions were invariably bimodal containing a low intensity fast mode deriving in part from internal modes, together with a dominant peak whose amplitude accounted at angle 90° for more than 90% of the scattered intensity. It is important to emphasize that, not only is there no aggregate peak, but also the static light scattering dependence of the reduced scattered intensity (KC/R_θ) is linearly dependent on $\sin^2(\theta/2)$ for each of the samples employed in the concentration range examined. These observations demonstrate that the scattering intensity is due only to the single coil and is not in part because of the presence of a slow mode as is usually the case with PEO solutions.

The dependence of the relaxation rates on the square of the scattering vector, q^2, is shown in Fig. 4. The fast mode at finite q in all cases is known to contain a contribution both

from translational diffusion as well as the first internal mode. We obtain from the intercept of the fast mode at zero q, $(2/\tau_1)$, an approximate value for the latter quantity of $\tau_1 = 0.6$ ms. This is of the same magnitude as observed for PS ($M = 3.8.10^6$) in toluene (0.4 ms) [6].

The slower peak was shown to be diffusive from the linear plots of relaxation rate Γ_θ versus $\sin^2(\theta/2)$; the translational diffusion coefficient (D) was determined by first extrapolating Γ_θ/q_θ^2 to zero angle; q_θ is the scattering vector at angle θ (Fig. 5). $D_{\theta=0}$ was then plotted against concentration and extrapolated to zero concentration (Fig. 6). Hydrodynamic radii were evaluated using Eq. (5). Parameters evaluated from SLS and DLS are summarized in Table 2.

As seen from Table 2, the magnitude of R_g, R_h and A_2 are generally higher than those for other linear flexible polymer chains in good solvents; see Refs. [1,2].

The power law fits between R_g and R_h and molecular weight are given by Eqs. (6) and (7)

$$R_g \sim M_w^{\nu} g \tag{6}$$

$$R_h \sim M_w^{\nu} h \tag{7}$$

Theoretically predicted values of ν_g and ν_h are 0.588 and 0.571, respectively [7–9]. The scaling exponent observed here for R_h is $\nu_h = 0.59$, which is in excellent agreement with that given in Refs. [1,2] for experimental data. However, the scaling exponent for R_g was found to be considerably lower (0.39) than anticipated (0.588). The deviant behavior is shown in Fig. 7 where R_g and R_h are plotted as functions of M_w. The R_g curve consequently tends to cross that for R_h in the high molecular weight limit, indicating formation of an increasingly compact particle. The deviation of R_g from the expected power law leads to a lower value of the ratio $\rho = R_g/R_h$ (Fig. 8) with increasing molecular weight, in contrast to the constant value of approximately 1.86 predicted, and usually observed, for highly swollen polymer coils [10]. Devanand and Selser [2] found a mean value of $\rho = 1.73$ for a series of PEO in the molecular weight interval up to 1×10^6. Our value for N750 of lowest molecular weight ($M_w = 0.64 \times 10^6$), $\rho = 1.8$, is in good agreement with the theoretical prediction. We note that similar behavior has been found for cellulose 2,5-acetate in acetone and THF, carboxymethyl cellulose in 1 M NaCl aqueous solution and for other aqueous and organic solvent solutions of various cellulose ethers [11–13]. There it was observed that the ρ-parameter typically decreases from the value for a flexible coil at $M \simeq 10^6$ to that

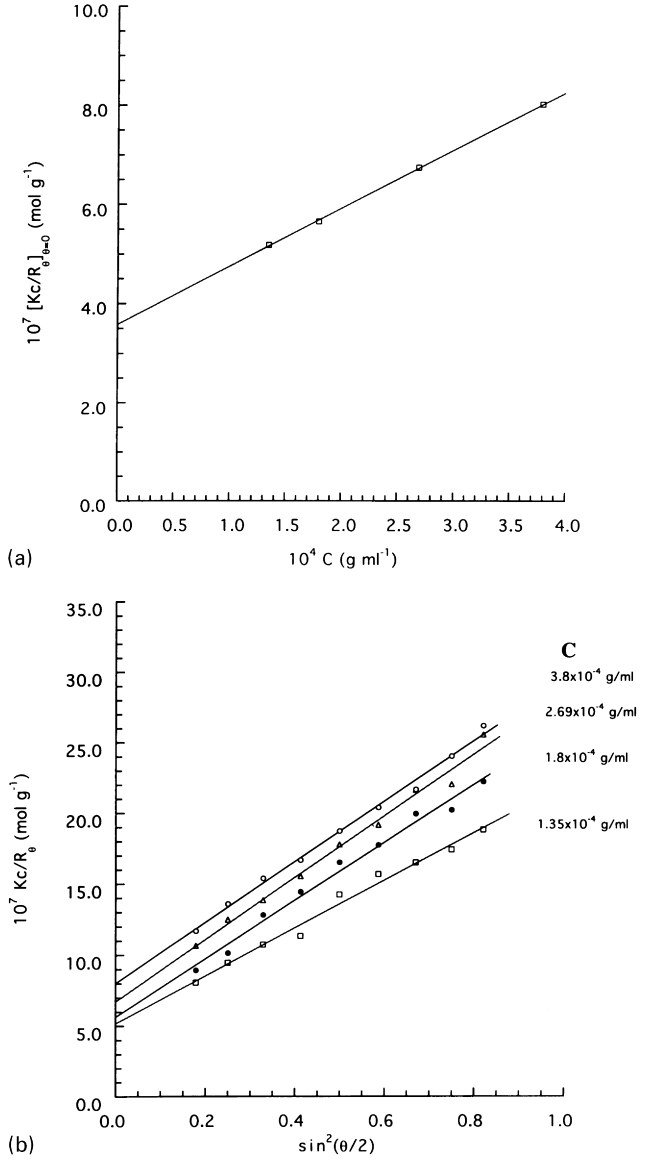

Fig. 1. (a) and (b) Static light scattering data for poly(ethyleneoxide) sample WSR ($M_w = 2.2 \times 10^6$).

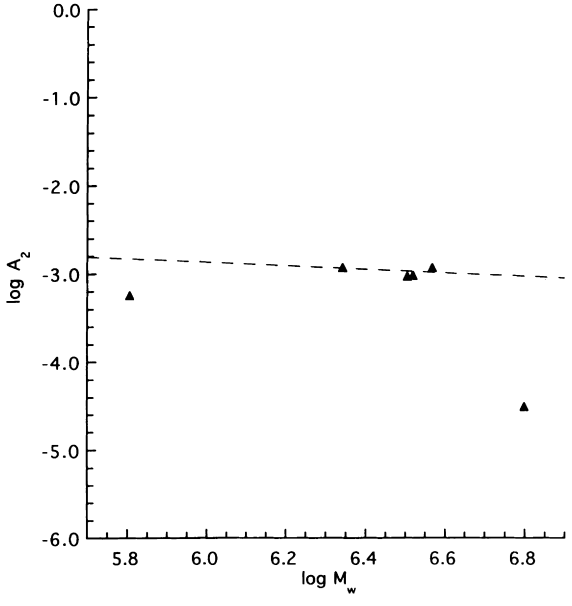

Fig. 2. Double logarithmic plot of second viral coefficient (A_2) versus molar mass.

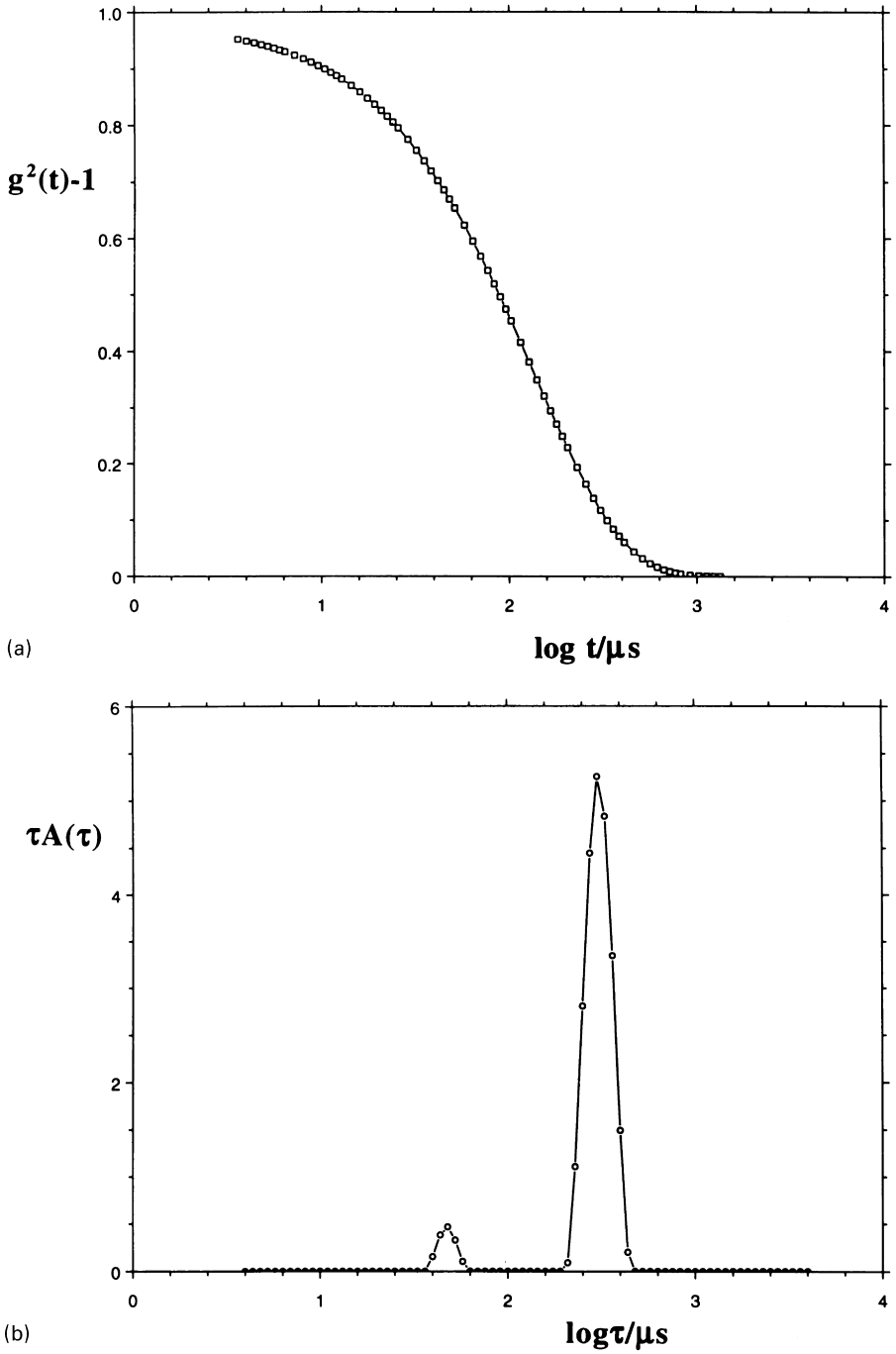

Fig. 3. (a) Time Correlation function for sample WSR ($M_w = 2.2 \times 10^6$) at $C = 0.896 \times 10^{-4}$ g ml^{-1}, angle 90° and 25°C. (b) Corresponding inverse Laplace transform of data in (a).

Table 2
Static and dynamic light scattering parameters for PEO samples

Sample	$10^{-6} M_w$ (g mol^{-1} (SLS))	R_g(nm (SLS))	$10^3 A_2$ (mol ml g^{-2} (SLS))	$10^{11} D_0$ (m^2 s^{-1} (DLS))	R_h (nm (DLS))	Ψ
N750	0.64	50.2	0.6	0.872	27.7	0.138
N12K	3.2	85.5	0.9	0.331	73.0	1.136
N60K	3.3	94.5	1.0	0.322	75.1	0.924
WSR 301	3.7	93.6	1.3_5	0.320	75.5	1.679
WSR	2.2	84.7	1.1_7	0.381	63.3	0.694
309	6.3	117.3	0.03	0.215	112.5	0.057

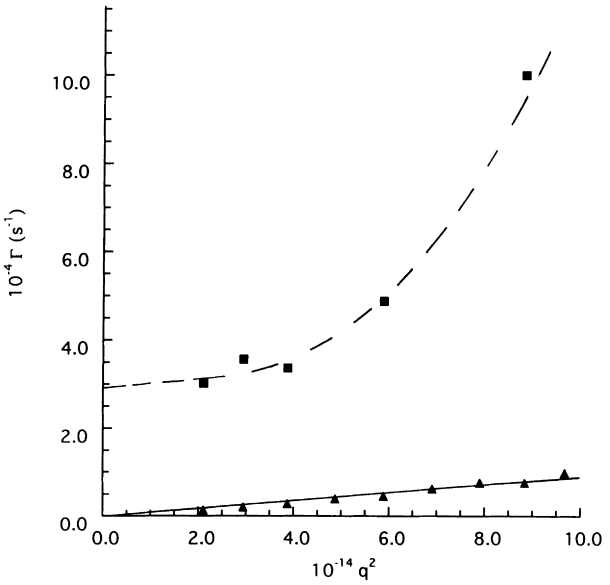

Fig. 4. Relaxation rates (Γ) as a function of a squared scattering vector for the fast and slow modes (see Fig. 3b).

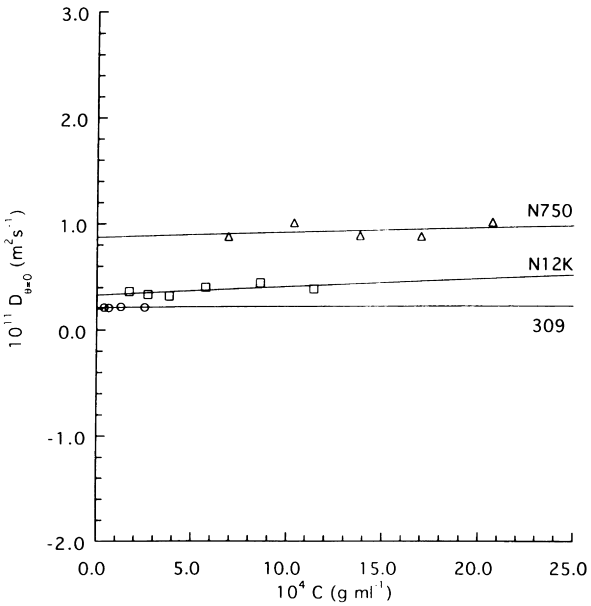

Fig. 6. Concentration dependence of diffusion coefficients for three PEO samples.

consistent for a hard sphere at above 10×10^6. The interpretation placed upon the low scaling exponent for R_g and the low values for ρ was formation of an intramolecularly crosslinked microgel. This is shown schematically in Fig. 9. The right hand side represents a single coil, which is intramolecularly crosslinked by hydrogen bonds mediated by water molecules, and the left-hand side depicts the analogous randomly coiled flexible chain.

The last column in Table 2 gives the values of the interpenetration parameter Ψ [2,14–16], which is frequently used to assess the extent of interpenetration of polymer coils in binary encounters and which is defined as:

$$\Psi = A_2 M_w^2 / 4\pi^{3/2} N_A R_g^3 \quad (8)$$

where A_2 is the second virial coefficient. Ψ is seen to be higher in value than typically found for other polymer/good solvent systems ($\Psi = 0.27$) [17,18], again reflecting the weak increase of R_g with M_w. The very low value of the second virial coefficient with the highest molecular mass sample is in keeping with the microgel model for the coupled chains.

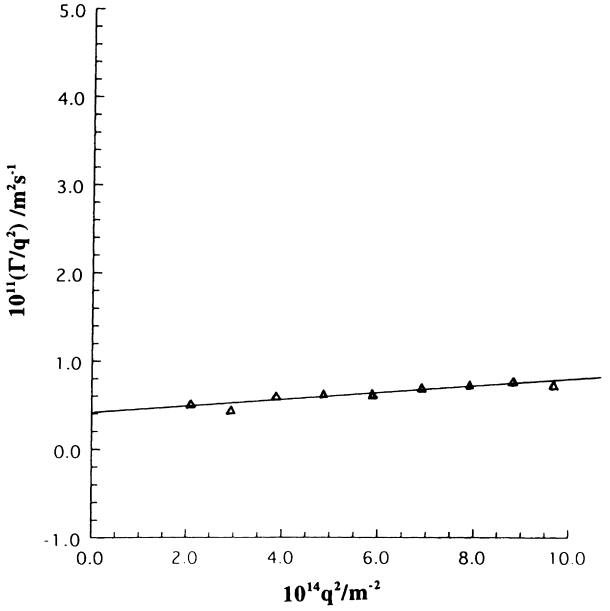

Fig. 5. Wave vector dependence of the apparent diffusion coefficient for sample WSR ($M_w = 2.2 \times 10^6$) ($C = 0.896 \times 10^{-4}$ g ml^{-1}) at 25°C.

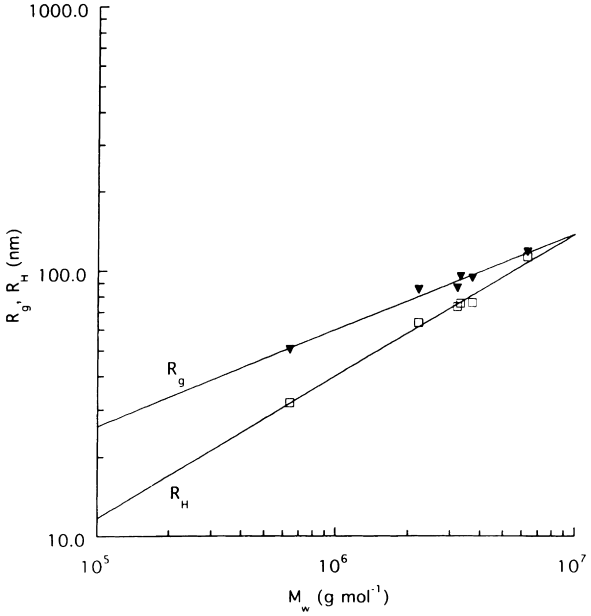

Fig. 7. Molecular weight dependence of radius of gyration and hydrodynamic radius for high molecular weight PEO samples.

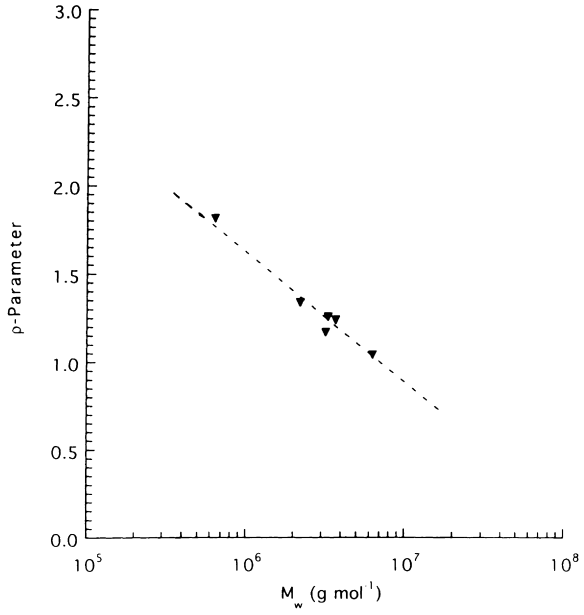

Fig. 8. Molecular weight dependence of the ρ-parameter ($= R_g/R_h$) for high molecular weight PEO samples.

4. Conclusions

Six commercial high molecular weight PEO samples were characterized by simultaneous static and dynamic light scattering. The radii of gyration (R_g), the second virial coefficients (A_2), the diffusion coefficients (D_z), and the hydrodynamic radii (R_h) were determined for the single coil in dilute solution. R_g, A_2, and R_h are generally larger than those determined for typical linear flexible polymer chains in good solvents. It was found that the anticipated power law behavior is observed for the hydrodynamic radius (0.59) but the scaling exponent for the radius of gyration is 0.39.

The PEO chain apparently follows expected patterns of behavior for a flexible chain in a good solvent up to molecular weights of about 0.6×10^6. At higher molecular weights, however, a strong deviation is found and the characteristic ratio ($\rho = R_g/R_h$) has a value of close to unity, instead of about 1.8 typifying the well-expanded coil. It would appear that PEO coils of very high molar mass undergo microgel formation and collapse into a more compact structures probably stabilized by intramolecular hydrogen bonding mediated through water molecules.

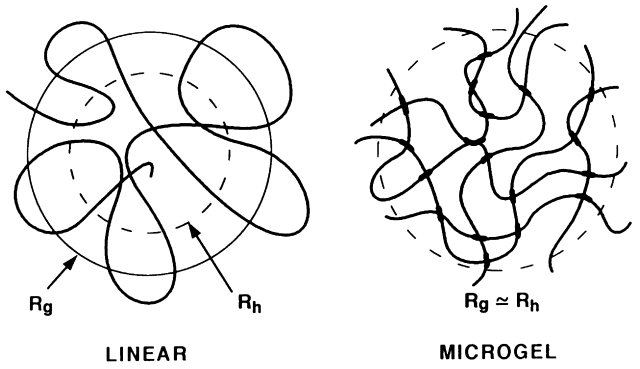

Fig. 9. Schematic diagram for a linear coil (left) and a microgel particle (right).

Acknowledgements

S.R. thanks the Swedish Institute for providing a grant supporting his stay in Sweden. Union Carbide Corporation are gratefully acknowledged for supplying the poly(ethyleneoxide) samples.

References

[1] Cotts PM, Selser JC. Macromolecules 1990;23:2050.
[2] Devanand K, Selser JC. Macromolecules 1991;24:5943.
[3] Schillén K, Brown W, Johnsen RM. Macromolecules 1988;27:4825.
[4] Chu B. Laser light scattering, 2. New York: Academic Press, 1991.
[5] Jakes J, Czech J Phys B 1988;38:1305.
[6] Nicolai T, Brown W, Johnsen RM. Macromolecules 1989;22:2795.
[7] Flory PJ. Principles of polymer chemistry, Ithaca, NY: Cornell University Press, 1953.
[8] Le Guillou J, Zinn-Justin C. J Phys Rev Lett 1977;39:95.
[9] Weill G, des Cloizeaux J. J Phys (Paris) 1979;40:99.
[10] Benmouna M, Akcasu AZ. Macromolecules 1980;13:409.
[11] Burchard W, Schultz L. Das Papier 1989;43:665.
[12] Burchard W, Schultz L. Das Papier 1992;47:1.
[13] Burchard W. Das Papier 1994;48:755.
[14] Yamakawa H. Modern theory of polymer solutions, New York: Harper and Row, 1971.
[15] Stockmayer WH. Makromol Chem 1960;35:54.
[16] Cotton PJ. J Chem Phys 1980;41:L231.
[17] Berry GC. J Chem Phys 1966;44:4550.
[18] Norisuye T, Kuwahara K, Teramoto A, Fujita H. J Chem Phys 1968;49:4330.